**Mathematical Biology**

Y. Dolak · T. Hillen

# Cattaneo models for chemosensitive movement

## Numerical solution and pattern formation

**Abstract.** We derive models for chemosensitive movement based on Cattaneo's law of heat propagation with finite speed. We apply the model to pattern formation as observed in experiments with *Dictyostelium discoideum*, with *Salmonella typhimurium* and with *Escherichia coli*. For *Salmonella typhimurium* we make predictions on pattern formation which can be tested in experiments. We discuss the relations of the Cattaneo models to classical models and we develop an effective numerical scheme.

## 1. Introduction

In this paper, we apply Cattaneo's law of heat propagation with finite speed ([4]) to the biological phenomenon of chemotaxis, or more generally, to chemosensitive movement. Chemosensitive movement describes the active orientation of individuals along chemical signals which are produced by the population itself. The most prominent examples of chemotactic species are the slime mold *Dictyostelium discoideum* (*Dd*), which moves towards higher concentrations of cAMP (cyclic adenosine mono-phosphate), or flagellated bacteria like *Salmonella typhimurium* (*St*), which reacts to aspartate.

In biological literature there is a distinction between chemotaxis and chemokinesis (see [29] or [6]). Whereas chemotaxis denotes a directed orientation towards or away from the chemical stimulus, chemokinesis describes some non-directed bias in the movement behavior, which indirectly leads to an oriented movement of the population. Chemokinesis appears in bacteria, who reduce their turning frequency while moving in a favorable direction. From a modeling point of view the above distinction is not necessary and we summarize all these orientation effects in *chemosensitive movement* (see a detailed discussion in [14]).

The classical mathematical model for chemosensitive movement is the Patlak-Keller-Segel model ([25], [19]). This model assumes diffusion of the species at hand. The purpose of this paper is to study an alternative model – a Cattaneo model – which respects finite propagation speeds and which is based on the individual movement patterns of the species.

Y. Dolak: TU Wien, Institut für Angewandte und Numerische Mathematik, Wiedner Hauptstr. 8-10, 1040 Wien, Austria. e-mail: yasmin.dolak@tuwien.ac.at

T. Hillen: University of Alberta, Department of Mathematical and Statistical Sciences, Edmonton, T6G 2G1, Canada. e-mail: thillen@ualberta.ca

In the following sections we apply the Cattaneo-chemotaxis model to experiments of Firtel [8] for the slime mold *Dictyostelium discoideum*, to experiments of Woodward *et al.* [30] for *Salmonella typhimurium* and to Ford's data [10,9] on *Escherichia coli*, using as many realistic parameters as possible.

We use the remainder of this introduction to explain, in detail, the appearence of the Cattaneo law from heat transport and from random walk processes. Since the Cattaneo model is a hyperbolic system it is worthwhile to discuss the numerical scheme which we developed to solve the equations. An appendix contains the discussion of the numerics.

### 1.1. Cattaneo's law

The *Cattaneo law* was introduced by C. Cattaneo in 1948 as a modification of Fourier's law of heat conduction. It is used to describe heat propagation with finite speed. In that context, let $\theta(t, x) \in \mathbb{R}$ denote the temperature of a homogeneous medium $\Omega \subset \mathbb{R}^n$ and let $q(t, x) \in \mathbb{R}^n$ denote the heat flux. Then the Cattaneo law, together with an equation for conservation of energy, leads to the *Cattaneo system* [4], [18]

$$\theta_t + \nabla \cdot q = 0, \qquad \tau q_t + q = -D\nabla\theta. \tag{1}$$

The constant $\tau > 0$ describes the adaptation time of the heat flux $q$ to the negative gradient of the temperature $\theta$. The parameter $D > 0$ is the diffusion constant. For $\tau = 0$ we obtain Fourier's law $q = -D\nabla\theta$ and system (1) translates into the heat equation $\theta_t = D\Delta\theta$. As shown by Gurtin and Pipkin [11], the Cattaneo law describes a flux which depends exponentially on the history of the temperature gradient. We observed, moreover, that the Cattaneo system (1) is the minimizing flux of an exponentially weighted Dirichlet integral. Define

$$F(\theta) := \frac{D}{2\tau} \int_0^t \int_\Omega e^{(s-t)/\tau} |\nabla\theta|^2 dx ds$$

then the first variation of $F$ is

$$\delta F(\theta) = \frac{D}{\tau} \int_0^t e^{(s-t)/\tau} \nabla\theta \, ds.$$

Hence $\delta F$ satisfies a Cattaneo law:

$$\tau(\delta F)_t + \delta F = -D\nabla\theta.$$

If $\theta$ is given by the minimizing flux equation $\theta_t = -\nabla \cdot \delta F$ of the functional $F$ then $(\theta, \delta F)$ solves the Cattaneo system (1).

In 1995, Hadeler [12] observed that the Cattaneo model is also useful for describing biological populations. In one space dimension, the Cattaneo system (1) is equivalent to the Goldstein-Kac model for a correlated random walk (see [12], [13]). In more than one space dimension we assume that $u(t, x) \in \mathbb{R}$ is a particle

density and that $v(t, x) \in \mathbb{R}^n$ describes a particle flux. The corresponding Cattaneo model is

$$u_t + \nabla \cdot v = 0, \qquad \tau v_t + v = -D\nabla u. \qquad (2)$$

The advantage of Cattaneo models is that the undesired feature of infinite fast propagation of information is omitted, as might occur in diffusion based models.

The semilinear Cattaneo system

$$u_t + \nabla \cdot q = f(u)$$
$$\tau q_t + q = -D\nabla u \qquad (3)$$

has been studied in Hillen [13] on bounded domains in $\mathbb{R}^n$ with smooth boundaries. The function $f$ describes birth and death of a population. The system has been studied with both homogeneous Dirichlet and homogeneous Neumann boundary conditions. With construction of a Lyapunov function it has been shown that, under appropriate growth assumptions on $f$, the $\omega$-limit sets are contained in the set of stationary solutions.

In Hillen [14], the Catteno system has been derived from a moment closure approach of transport equations. For that, consider bacteria which move according to the following rules (as observed by Berg [1] and many others): An individual cell moves with nearly constant speed in a certain direction. It suddenly stops, rotates and chooses a new direction at random. The stopping times can be modeled by an exponential distribution with rate $\mu$. The rotation-times are small compared to periods of movement. The distribution of new chosen directions (preferred turn-angles) can be measured in experiments. It is denoted by $T(v, v')$, where $v', v \in V$ are incoming and outgoing velocity, respectively. The set $V \subset \mathbb{R}^n$ is the set of possible velocities and, in this case, we have $V = sS^{n-1}$, where $s$ is the cell speed. Stroock [28] has shown that this process (in an appropriate limit) leads to a linear transport equation

$$p_t + v \cdot \nabla p = -\mu p + \mu \int T(v, v') p(v') dv', \qquad (4)$$

where $p(t, x, v)$ denotes the particle density at time $t \geq 0$ at spatial position $x \in \Omega$ of particles moving with velocity $v \in V$. Transport models and related stochastic processes have also been discussed in Othmer *et al.* [23]. To derive the Cattaneo system we assume that the cells have no preferred turn-angle, i.e. $T(v, v') = |V|^{-1}$ is constant. Then (4) describes a Pearson walk [26].

We introduce the velocity moments of $p$

$$m_0(t, x) := \int_V p(t, x, v) dv$$

$$m_i(t, x) := \int_V v_i p(t, x, v) dv, \quad i = 1, \ldots, n$$

$$m_{ij}(t, x) := \int_V v_i v_j p(t, x, v) dv, \quad i, j = 1, \ldots, n.$$

Multiplication of (4) with 1 or $v_i$ for $i = 1, \ldots, n$ and integration along $V$ leads to a system for the first two moments:

$$m_{0,t} + \sum_{i=1}^{n} \partial_i m_i = 0 \tag{5}$$

$$m_{i,t} + \sum_{j=1}^{n} \partial_j m_{ij} = -\mu m_i, \tag{6}$$

where $\partial_i = \frac{\partial}{\partial x_i}$. As thoroughly illustrated in Hillen [14] the above moment system can be closed for $(m_0, m_1, \ldots, m_n)$ by minimizing the $L^2(V)$-norm:

$$H(u) := \frac{1}{2} \int_{\Omega} u^2 dx$$

with constraints

$$\int u(t, x, v) dv = m_0(t, x) \tag{7}$$

and

$$\int v_i u(t, x, v) dv = m_i(t, x), \quad i = 1, \ldots, n. \tag{8}$$

The minimizer can explicitly be given as

$$u_{\min}(t, x, v) = \frac{1}{|V|} \left( m_0(t, x) + \frac{n}{s^2} \sum_{i=1}^{n} v_i m_i(t, x) \right).$$

We assume that the second moment $m_{ij}(p)$ of $p$ is well approximated by the second moment of the minimizer $u_{\min}$. Then the closed system reads (see [14])

$$M_{0,t} + \sum_{i=1}^{n} \partial_i M_i = 0$$

$$M_{i,t} + \frac{s^2}{n} \partial_i M_0 = -\mu M_i, \quad i = 1, \ldots, n \tag{9}$$

where we used capital letters to distinguish from the true moments $m_0, m_i$. Note that (9) is indeed a Cattaneo system (1). The error which appears during this approximation can be controlled (see [14]).

## 1.2. Boundary conditions

If we study Cattaneo models on bounded domains, the boundary conditions have to be considered carefully. We can use the minimizer $u_{\min}$ of the previous section to translate boundary conditions of the transport model into boundary conditions of the Cattaneo system.

The homogeneous Dirichlet boundary condition for the transport equation (4) is:

$p(t, x, v) = 0$ *for all* $x \in \partial\Omega$ *and all* $v \in V$ *with* $v \cdot \eta(x) < 0$, *where* $\eta(x)$ *denotes an outer normal at* $\partial\Omega$.

Here we assume that the boundary of $\Omega$ is piecewise differentiable. If $x \in \partial\Omega$ allows for more than one outer normal vector (corner points), we require the above condition for all outer normals.

It is natural to assume that the minimizer $u_{\min}$ satisfies the same boundary condition. This leads directly to

$$m_0 = \frac{2nK_V}{s^2|V|}\eta(x) \cdot \vec{m}, \tag{10}$$

with

$$K_V := \int_{\{v \in V: v_1 \geq 0\}} v\, dv \cdot e_1,$$

where $\vec{m} = (m_1, \ldots, m_n)$ and $e_1 = (1, 0, \ldots, 0)$. For $V = sS^{n-1}$ we explicitly calculate the constants $K_V$: For $n = 1$ we have $K_V = s$, for $n = 2$ we obtain $K_V = 2s$ and for $n \geq 3$ we get

$$K_V = s^{n-1}\int_{\{\sigma \in S^{n-1}:\sigma_1 \geq 0\}} \sigma\, d\sigma \cdot e_1 = s^{n-1}\int_{S^{n-2}}\int_{-\pi/2}^{\pi/2} \cos\varphi\, d\varphi\, d^{n-2}\omega,$$

where $d^{n-2}\omega$ denotes the surface measure on $S^{n-2}$. Then

$$K_V = 2s^{n-1}|S^{n-2}|.$$

The factor which appears in the boundary conditions is then given as

$$\frac{2nK_V}{s^2|V|} = \begin{cases} s^{-1} & \text{for } n = 1, \\ 4(s^2\pi)^{-1} & \text{for } n = 2, \\ 4ns^{-2}|S^{n-2}|/|S^{n-1}| & \text{for } n \geq 3. \end{cases}$$

For the modeling of chemotaxis we use homogeneous Neumann boundary conditions. If we start again with pure physical reflection conditions for the transport model (4) we have

$$v \cdot \vec{m} = (v - 2(\eta(x) \cdot v)\eta(x)) \cdot \vec{m}$$

for all velocities $v$ with $v \cdot \eta(x) < 0$. This reduces to

$$\eta(x) \cdot \vec{m} = 0. \tag{11}$$

### 1.3. Models for chemosensitive movement

Before we derive detailed models for *Dd* and *St*, we explain the basic modeling assumptions and we illustrate the relations to the classical Patlak-Keller-Segel model (PKS-model). The PKS-model in a simple form reads

$$u_t = \nabla(D_u\nabla u - V(u, S)\nabla S)$$
$$S_t = D_S\Delta S + g(u, S),$$

where $u(t, x)$ denotes the cell density and $S(t, x)$ the signal concentration. The function $V(u, S)$ is a (nonlinear) cross-diffusion coefficient. The function $g(u, S)$ describes production and degradation of the signal. Many authors studied qualitative properties of this system for $V(u, S) = u\chi(S)$ and $g(u, S) = -\nu S + \alpha u$. Results on finite time blow-up are known (see the references in [16] or in [14]).

In Hillen and Painter [16], the chemotactic cross diffusion $V$ is chosen as $V(u, S) = u\beta(u)\chi(S)$, where $\beta(u)$ describes density control ($\beta(0) > 0$, $\beta(\bar{u}) = 0$ for some $\bar{u} > 0$ and $\beta(u) > 0$ for all $0 < u < \bar{u}$) and $\chi(S) \geq 0$ is the *chemotactic sensitivity*. For this choice of $V$ solutions exist globally in time, and spatial patterns can be observed (see [16]). Here we aim to use the density control ansatz for the Cattaneo model as well.

There are, at least, two ways to derive the corresponding Cattaneo model for chemosensitive movement. Heuristically, we consider the population-flux of the PKS-model

$$q = -D_u \nabla u + V(u, S)\nabla S. \tag{12}$$

Again we assume that the flux $q$ is not instantaneously equal to the right hand side of (12), but it relaxes to it with a time constant $1/\tau$. Then the corresponding *Cattaneo model for chemosensitive movement* reads

$$u_t + \nabla \cdot q = 0$$
$$\tau q_t + q = -D_u \nabla u + V(u, S)\nabla S. \tag{13}$$

As shown in Hillen [14], we can also derive (13) from an associated transport model, where turning rate and turning kernel $T$ are chosen appropriately. For example, we chose

$$\mu(m_0, v; S, \nabla S) := \mu_0 \left(1 - \frac{n}{s^2} V(m_0, S)v \cdot \nabla S\right) \tag{14}$$

and

$$T(v, v'; S, \nabla S) := \frac{1}{|V|}\mu(m_0, v'; S, \nabla S), \tag{15}$$

with $V = s S^{n-1}$ and $m_0(t, x) = \int_V p(t, x, v)dv$ as before. The moment closure procedure applies and leads to (13) (see [14]).

## 2. A model for slime molds

The slime mold *Dictyostelium discoideum* has developed an extraordinary mechanism: upon starvation, the amoebae form tissue-like aggregates. This process is controlled by chemotaxis; the cells move upward gradients of the messenger molecule cAMP produced by the cells themselves. Eventually, they form a fruiting body, where spores can survive until conditions for germination are favorable.

The formation of aggregates has been documented by many authors. We are guided by observations of Firtel *et al.*[8]. The aim of our simulations is not to

reproduce the experimental results as precisely as possible, but to describe them qualitatively. The model equations are:

$$\tilde{u}_{\tilde{t}} + \widetilde{\nabla} \cdot \tilde{q} = 0 \tag{16}$$

$$\tau \tilde{q}_{\tilde{t}} + \tilde{q} = -D_u \widetilde{\nabla} \tilde{u} + \chi \tilde{u} \left(1 - \frac{\tilde{u}}{K}\right) \widetilde{\nabla} \tilde{S} \tag{17}$$

$$\tilde{S}_{\tilde{t}} = D_s \widetilde{\Delta} \tilde{S} + k_1 \tilde{u} - k_2 \tilde{S}. \tag{18}$$

Here we use $\tilde{u}$, $\tilde{q}$, and $\tilde{S}$ for the particle density, the particle flux, and the signal concentration, respectively. Later we use expressions without ~ for the corresponding non-dimensional variables. We model the chemotactic cross diffusion with a simple logistic law $V(\tilde{u}, \tilde{S}) = \chi \tilde{u}(1 - \frac{\tilde{u}}{K})$, where $K$ is the maximal cell density. The chemotactic sensitivity $\chi$ is assumed to be constant $> 0$. Moreover, we assume linear production and degradation of the chemoattractant $\tilde{S}$ with $k_1, k_2 > 0$.

To non-dimensionalize the system, we choose the following scaling:

$$t = \frac{\tilde{t}}{t_0}, \quad x = \frac{\tilde{x}}{x_0}, \quad \text{with} \quad t_0 = k_2^{-1}, \quad x_0 = \sqrt{D_s k_2^{-1}}. \tag{19}$$

The dimensionless variables $u(x, t)$, $q(x, t)$ and $S(x, t)$ are given by $u = \tilde{u} K^{-1}$, $q = \tilde{q} K^{-1} (D_s k_2)^{-\frac{1}{2}}$ and $S = \tilde{S} \chi D_s^{-1}$. Thus we obtain the equations

$$u_t + \nabla \cdot q = 0 \tag{20}$$
$$\tau q_t + q = -D \nabla u + u(1 - u) \nabla S \tag{21}$$
$$S_t = \Delta S + \alpha u - S. \tag{22}$$

The parameter values are listed in Table 1 and 2. For those parameters not available in the literature, we choose reasonable values. The non-dimensionalized system depends only on $\tau$, $D$ and $\alpha$. The numerical values are given below each of the figures Fig. 1 and 2, respectively.

We impose Neumann boundary conditions on a bounded domain $\Omega$ (petri-dish). For the chemical concentration $S$ it is given as

$$\nabla S \cdot \eta \quad |_{\partial \Omega} = 0. \tag{23}$$

The boundary condition for the population-flux $q$ has been already derived in Section 1.2. It reads

$$q \cdot \eta \quad |_{\partial \Omega} = 0. \tag{24}$$

**Table 1.** Parameters of the non-dimensional model (20)–(22).

| Non-dimensional parameter | Definition |
| --- | --- |
| $\tau$ | $k_2 \tilde{\tau}$ |
| $D$ | $D_u D_s^{-1}$ |
| $\alpha$ | $\chi K k_1 (k_2 D_s)^{-1}$ |

**Table 2.** Dimensional parameter values used in eq. (16)–(18). The time constant $\tau$ corresponds to the average duration of cell movement. In [7], the diffusivity of cAMP was measured in water; we take 75% of this value for diffusion on agar ($D_s = 3 \times 10^{-6} \text{cm}^2 \text{ s}^{-1}$). Assuming a correlated random walk, the cell diffusion coefficient, $D_u$, is given by $\frac{s^2 \tilde{\tau}}{2}$. With $s = 2.5 \times 10^{-5} \text{cm s}^{-1}$ and $\tilde{\tau} = 320$ s, we obtain $D_u = 1 \times 10^{-7} \text{cm}^2 \text{ s}^{-1}$.

| Parameter | Experimental value | Reference |
|---|---|---|
| cell speed $s$ | $2 - 2.5 \times 10^{-5} \text{cm s}^{-1}$ | Rietdorf *et al.* [27] |
| time constant $\tilde{\tau}$ | 240 - 360 s | Rietdorf *et al.* [27] |
| $\chi$ | no measurements available | |
| $D_s$ | $4 \times 10^{-6} \text{cm}^2 \text{ s}^{-1}$ | Dworkin and Keller [7] |
| $k_1, k_2$ | no measurements available | |
| $K$ | $10^5 - 10^6 \text{ cells cm}^{-2}$ | |
| $D_u$ | $1 \times 10^{-7} \text{cm}^2 \text{ s}^{-1}$ | |



(a) $t = 250$
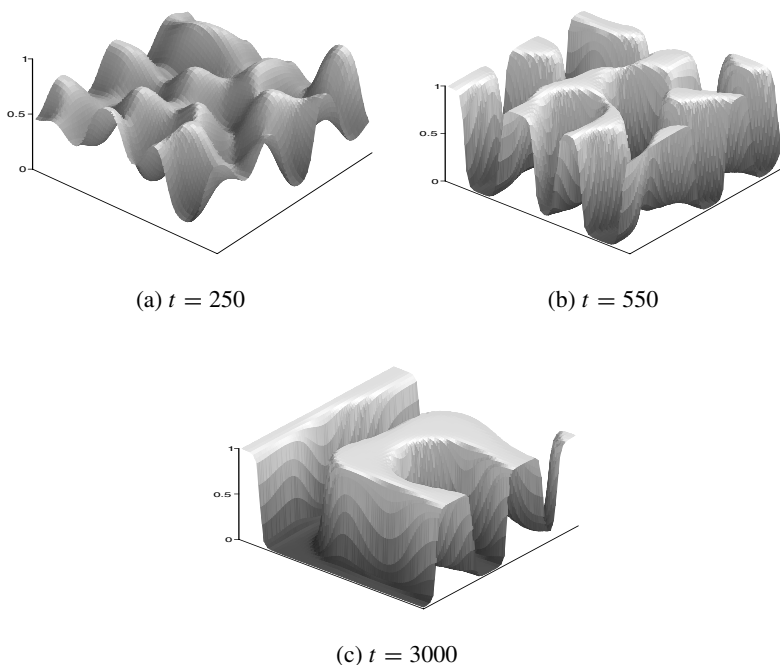


(b) $t = 550$



(c) $t = 3000$

**Fig. 1.** Numerical solution of the model (20)–(22) with initial condition $u(x, y) \in [0.5, 0.51]$ on a square domain $[0, 20]^2$. Parameter values: $D = 0.03$, $\tau = 1$, $\alpha = 0.5$.

The initial conditions are

$$u(\cdot, 0) = u_0, \quad q(\cdot, 0) = q_0, \quad S(\cdot, 0) = S_0. \tag{25}$$

## 2.1. Simulation results

We solve the Cattaneo system (20)–(22) with boundary conditions (23) and (24) on a bounded square domain $\Omega = [0, 20] \times [0, 20]$. The numerical scheme is
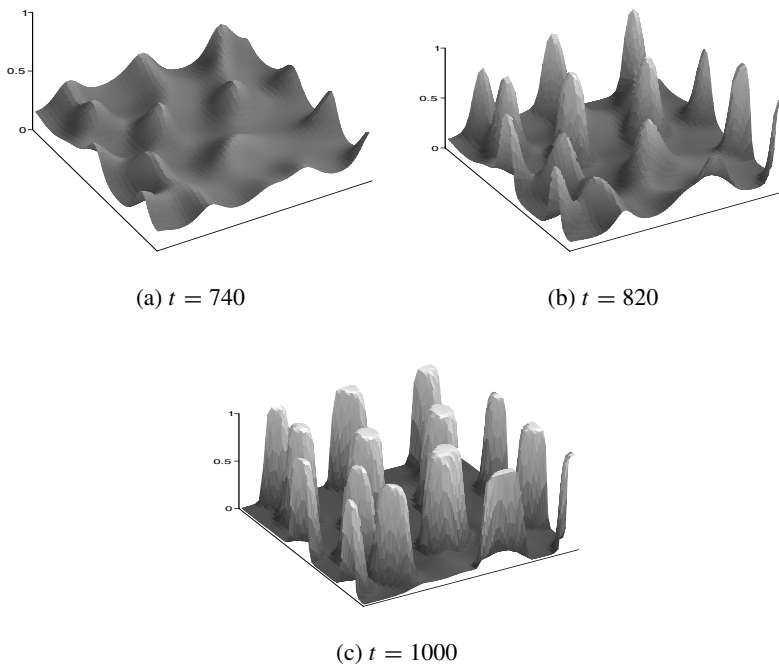
(a) $t = 740$                                        (b) $t = 820$



(c) $t = 1000$

**Fig. 2.** Numerical solution of the model (20)–(22) with initial condition $u(x, y) \in [0.2, 0.21]$ on a square domain $[0, 20]^2$. Parameter values: $D = 0.03$, $\tau = 1$, $\alpha = 0.8$.

discussed in the Appendix. In all simulations, the initial condition is a homogeneous distribution of the cell density with random fluctuations of 1%. The flux $q$ and the concentration of the chemical $S$ are zero initially.

In Fig. 1, we show the time evolution of the cell density $u$. The initial distribution is $u_0 = 0.5 + \text{random}$. Due to initial irregularities of the cell density, small aggregations start to form. We observe collision and collapse of peaks, a phenomenon which is known from simulations of corresponding parabolic models [16]. The aggregations continue to grow, until plateaus at $u = 1$ are formed. Eventually, they merge as well.

In Fig. 2, the initial distribution is $u_0 = 0.2 + \text{random}$. Compared to experiments made at Firtel-Lab of the University of California, San Diego [8], we see that the transition from many small maxima to a few large aggregations can be observed in both cases. However, it is apparently only possible to describe the experiments qualitatively. Since the experimental value of the parameter $k_2$ is not known, time and space scale of our model remain undetermined. For the scaling which we chose in (19), the time and space scales are coupled via $x_0 = \sqrt{D_s t_0}$. We choose the square domain $[0, 20]^2$ to correspond to the experimental domain. In reality, it takes about 8 hours until aggregates are formed (R. Firtel, personal communication). In our simulations, though, it takes much longer. The reason for this difference could be the fact that the model does not take into account the rather

complicated dynamics of cAMP production and the propagation of chemical waves (see e.g. [22]).

## 3. A model for bacteria

Under certain conditions, strains of the bacterium *Salmonella typhimurium* form ring-shaped or spotted patterns. In experiments of H.C. Berg and E. Budrene (see Woodward *et al.*[30]), a population of bacteria was inoculated at the centre of a petri dish filled with semi-solid agar and with a growth substrate. The population first spreads in a homogeneous form and produces a bacterial lawn. Later the cells start to form concentric rings, which at low concentrations of the substrate, immediately break apart into discrete arcs or spots. At higher initial concentration of the substrate, the rings remain intact. This type of pattern formation cannot be explained without chemotaxis.

Woodward *et al.*[30] have proposed a mathematical model for this mechanism based on the diffusion equation. We will introduce a Cattaneo model for this phenomenon, which includes population growth, chemotactic response, and production of the chemoattractant according to [30].

In contrast to the experiments with *Dd*, the cell population is not constant. We assume that the cells proliferate with a constant rate $k_1$, until a certain density, which depends on the substrate concentration, is reached. Since the part of the substrate which is consumed during the experiments is small, we consider the underlying substrate concentration to be constant $c > 0$. The equation for the cell density $u(t, x)$ then reads

$$\tilde{u}_{\tilde{t}} + \tilde{\nabla} \cdot \tilde{q} = k_1 \tilde{u} \left( 1 - \frac{\tilde{u}}{k_2 c} \right). \tag{26}$$

Again the population-flux is given by Eq. (13). We choose the function $V(u, S)$ as proposed by Lapidus and Schiller [20] in 1976. They studied experiments with *E. coli*, a closely related species to *St*:

$$\tilde{\tau} \tilde{q}_{\tilde{t}} + \tilde{q} = -D_u \tilde{\nabla} \tilde{u} + \frac{k_3 \tilde{u}}{(k_4 + \tilde{S})^2} \tilde{\nabla} \tilde{S}. \tag{27}$$

From experiments, we know that the production of aspartate is approximately linear in the cell density $u$ and the substrate concentration $c$. At high cell densities, the production saturates:

$$\tilde{S}_{\tilde{t}} = D_s \tilde{\Delta} \tilde{S} + \frac{k_5 c \tilde{u}}{k_6 + \tilde{u}} - k_7 \tilde{S}. \tag{28}$$

Here we choose a linear degradation of the chemical.

Again, we have to non-dimensionalize the model. With time scale $t_0 = k_7^{-1}$ and space scale $x_0 = D_s^{\frac{1}{2}} k_7^{-\frac{1}{2}}$, we obtain the following equations for the dimensionless

**Table 3.** Parameters of the non-dimensional model (29)–(31).

| Non-dimensional parameter | Definition |
|---|---|
| $\tau$ | $k_7\tilde{\tau}$ |
| $D$ | $D_u D_s^{-1}$ |
| $\rho$ | $k_1 k_7^{-1}$ |
| $\alpha$ | $k_2 k_3 k_5 (k_4^2 k_6 k_7 D_s)^{-1}$ |
| $\beta$ | $k_2 k_5 (k_4 k_6 k_7)^{-1}$ |
| $\gamma$ | $k_2 k_6^{-1}$ |

**Table 4.** Dimensional parameter values used in equ. (26)–(28). $k_1$ can be determined from the average cell doubling time, which is about 2h.

| Parameter | Experimental value | Reference |
|---|---|---|
| time constant $\tau$ | 1–10 s | Berg and Brown [2] |
| $D_u$ | $2$–$4 \times 10^{-6}$ cm$^2$ s$^{-1}$ | Berg and Turner [3], Berg [1] |
| $D_s$ | $8.9 \times 10^{-6}$ cm$^2$ s$^{-1}$ | Berg [1] |
| $k_1$ | $\approx 9.6 \times 10^{-5}$ s$^{-1}$ | Woodward et al. [30] |
| $k_2$ | no measurements available | |
| $k_3$ | $3.9 \times 10^{-9}$ M cm$^2$ s$^{-1}$ | Dahlquist et al. [5] |
| $k_4$ | $5 \times 10^{-6}$ M | Dahlquist et al.[5] |
| $k_5, k_6, k_7$ | no measurements available | |

variables $u = \tilde{u} k_2^{-1}$, $q = \tilde{q} k_2^{-1} (D_s k_7)^{-\frac{1}{2}}$ and $S = \tilde{S} k_6 k_7 (k_2 k_5)^{-1}$:

$$u_t + \nabla \cdot q = \rho u \left(1 - \frac{u}{c}\right) \tag{29}$$

$$\tau q_t + q = -D\nabla u + \frac{\alpha u}{(1 + \beta S)^2} \nabla S \tag{30}$$

$$S_t = \Delta S + \frac{cu}{1 + \gamma u} - S. \tag{31}$$

Like before, we use homogeneous Neumann boundary conditions (23) and (24).

### 3.1. Simulations for bacteria

We solve system (29)–(31) numerically and vary the substrate concentration $c$. Initial values are chosen corresponding to the experimental conditions: the cell density is 1.0 in a small circular area in the centre of the domain. Everywhere else, it is 0. The flux and the concentration of aspartate is initially zero everywhere. Fig. 3 shows the evolution of the cell density for two different substrate concentrations. The results are closely comparable to the experimental observations: at a low substrate concentration $c$ ((a) in Fig. 3), concentric rings are formed which later break into spots. At high substrate concentrations ((b) in Fig. 3), the chemotactic response is saturated and the rings remain intact. If we compare our simulations to the experiments, we can estimate the time scale $t_0 = 180$ s and the length scale $x_0 = \sqrt{D_s t_0}$ approximately 0.04 cm. Thus we get a time interval of 2.2 hours between the formation of successive rings, and a distance of 2.8 mm between the
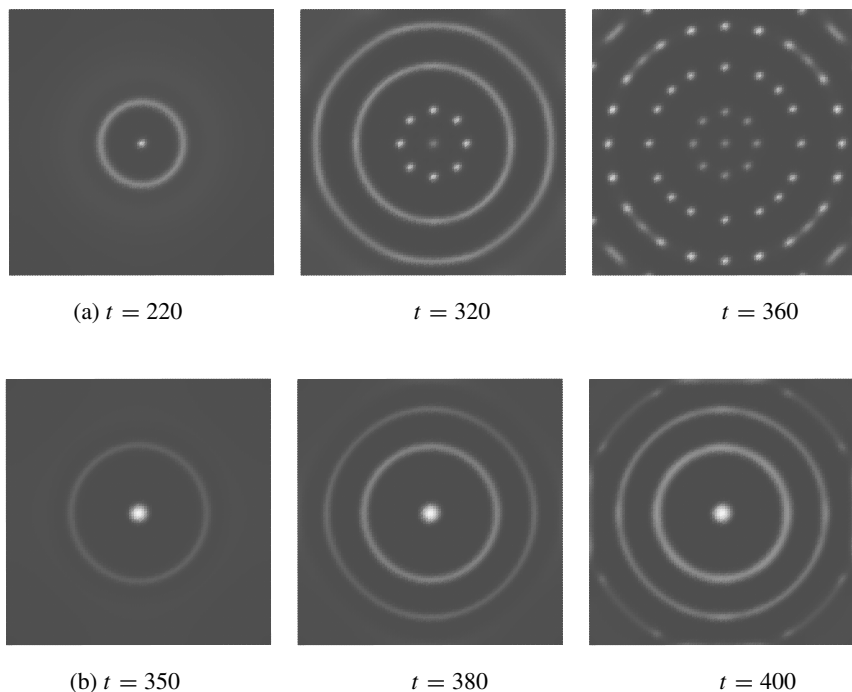
(a) $t = 220$             $t = 320$             $t = 360$

(b) $t = 350$             $t = 380$             $t = 400$

**Fig. 3.** Numerical solution of model (29)–(31) on a square domain $[0, 62]^2$. The evolution of the cell density at two different substrate concentrations is shown: in the top row (3(a)), the substrate concentration is $c = 0.8$, in the bottom row (3(b)), it is $c = 2.5$. Parameter values: $D = 0.3$, $\tau = 0.03$, $\beta = 2$, $\alpha = 9$, $\rho = 0.03$, $\gamma = 0.2$.

rings. These values compare well to the experimental results (around 2 hours and 2 mm, respectively).

We are interested in what happens if two competing ring-forming swarms overlap. We consider a numerical simulation, where the nutrient concentration is as in the ring-case above. Initially we inoculate the petri dish in two circular regions with a cell density of 1.0. In Figure 4 we show the developed pattern at time $t = 420$. We find that in the overlap region spots are formed and the rings are broken. This suggests, that the ring formation is an unstable mechanism compared to spot formation. Our computer prediction might be tested in experiments.

## 4. Discussion

In this article we discuss a model for chemosensitive movement, which is based on Cattaneo's law. In contrast to the classical Patlak-Keller-Segel model, which basically uses Fourier's law, the Cattaneo law accounts for finite propagation speeds of perturbations. Here the Cattaneo model (9) has been derived from a moment closure procedure of a kinetic equation. Using this approach, the relevant model parameters, such as $\tau$, $\gamma$, $V$ are directly related to the movement characteristics
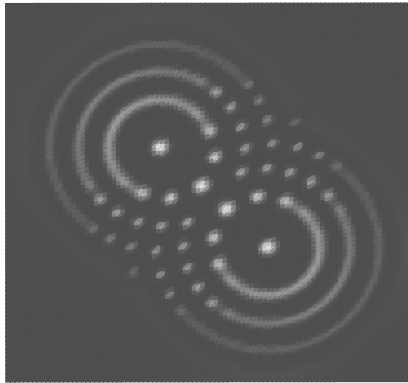
**Fig. 4.** Pattern generation of two competing swarms at time $t = 420$ on a domain of $[0, 118]^2$. The parameter values are as in Figure 3(b).

(i.e. turning rate $\mu$ and velocity distribution $T$) of the individuals at hand. Equations (13), (14) and (15) show one possible relation.

It is straightforward to include more detailed dependencies on space $x$, or on external factors like light sources, temperature gradients or variables which describe internal chemical pathways. For internal pathways in chemotaxis see the review article of Othmer and Schaap [24].

In the studies presented here, the Cattaneo model for chemosensitive movement is well suited to describe the experimentally observed patterns. We expect that the PKS model and the Cattaneo model for chemosensitive movement have the same asymptotic behavior. In one space dimension this has been considered in [17]. Hence on a long time scale we expect that both model classes (hyperbolic and parabolic) show the same results. For short time ranges, however, we expect a better description from a Cattaneo type model, due to finite characteristic speed. To investigate this we study the experiments on bacterial chemotaxis done by Ford *et al.* [10,9]. Due to symmetries of the experimental setup a one-dimensional model is appropriate. In Figures 4 and 7 of [10] the spatial spread is shown as a function of square-root of time. If the underlying process is pure diffusion, then the occupied area of the bacterial swarm should be proportional to the square-root of time, hence a linear fit gives a (mean) diffusion coefficient. For a correlated random walk, the spatial spread is proportional to time for short time ranges and proportional to the square-root of time for large time ranges (see [23]). Hence a graph corresponding to Figure 4 of [10] should be curved like a parabola near zero, eventually growing linearly. In Figure 5 we compare Ford's data with a linear fit, which corresponds to a diffusion model assumption and with a simulation of a one dimensional Cattaneo model [17].

We used realistic parameter values as given in Ford *et al.*, like a particle speed of $\gamma = 0.01$ mm/s and a turning rate of $\mu = 1\mathrm{s}^{-1}$ on a spatial domain of length 40 mm. We observe that both models, parabolic and hyperbolic, describe the data. Differences can be seen in the time range up to about 40 s. For Ford's experiments
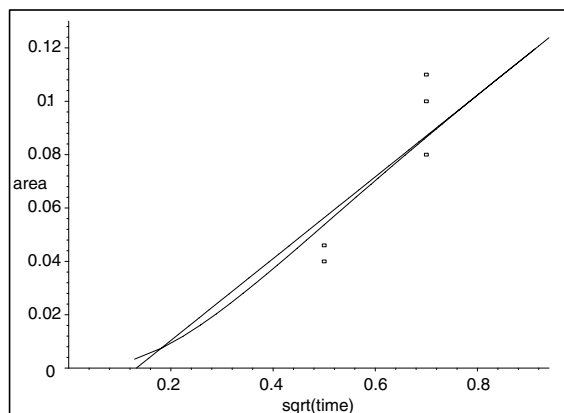
**Fig. 5.** Comparison of the experimental data of Ford *et al.* [10] (boxes) to a diffusion based model (linear curve) and to the simulation for a one-dimensional Cattaneo model (parabola-shaped line).

both model types are appropriate and we should choose the model according to the available data. If spread is measured for the population as a whole (motility $D$ or chemotactic sensitivity, $\chi$) then a diffusion based model should be used. If individual paths are followed and turning rates and turn-angle distributions are measured, then a hyperbolic model is more appropriate.

This, indeed, reflects the general outcome of our research. Depending on the available experimental parameters, a diffusion model is appropriate for population parameters and a transport model, or a Cattaneo model is advantageous if parameters for movement of individuals are available. There certainly is an overlap region, where both model types can be used with equal rights. From a more theoretical point of view, the transport- and Cattaneo-models provide a convenient platform to study and understand how the behavior of a population as a whole emerges from the behavior of its individual members.

## A. Numerical appendix

Since the Cattaneo system is hyperbolic, the numerical scheme has to be chosen carefully. To solve the model for slime molds, we use an algorithm based on the Lax-Wendroff scheme (see Section A.2). The numerical treatment of bacteria requires minor alterations of the slime molds-algorithm (Section A.3). First we consider the numerical boundary conditions (Section A.1).

### A.1. Numerical boundary conditions

Here, and for the following sections, we use standard notation: on a rectangular domain, we use mesh indices $i = 0, ..., I$ and $j = 0, ..., J$ with mesh width $h$ and time step $k$. We arrange the enumeration such that the domain boundaries are given by the indices $i = 1, I - 1$ and $j = 1, J - 1$, respectively. Mesh points with

index $i = 0$ or $I$ and $j = 0$ or $J$ are ghostpoints, which allows us to establish the boundary conditions in a simple way. In each time step, we define

$$u_{i,0}^n = u_{i,2}^n, \qquad u_{i,J}^n = u_{i,J-2}^n, \qquad i = 1, ..., I - 1 \qquad (32)$$

$$u_{0,j}^n = u_{2,j}^n, \qquad u_{I,j}^n = u_{I-2,j}^n, \qquad j = 1, ..., J - 1 \qquad (33)$$

$$S_{i,0}^n = S_{i,2}^n, \qquad S_{i,J}^n = S_{i,J-2}^n, \qquad i = 1, ..., I - 1 \qquad (34)$$

$$S_{0,j}^n = S_{2,j}^n, \qquad S_{I,j}^n = S_{I-2,j}^n, \qquad j = 1, ..., J - 1 \qquad (35)$$

$$q1_{0,j}^n = -q1_{2,j}^n, \qquad q1_{I,j}^n = -q1_{I-2,j}^n, \qquad j = 1, ..., J - 1 \qquad (36)$$

$$q2_{i,0}^n = -q2_{i,2}^n, \qquad q2_{i,J}^n = -q2_{i,J-2}^n, \qquad i = 1, ..., I - 1. \qquad (37)$$

The cornerpoints $u_{0,0}$, $u_{I,J}$, etc. are not used for the algorithm. Now the use of central differences for gradients at $i = 1, ..., I - 1$ and $j = 1, ..., J - 1$ leads to the exact fullfillment of the described boundary conditions (23) and (24). Note that from (21), (23), and (24) it follows that $u$ satisfies $\nabla u \cdot \eta = 0$ at $\partial\Omega$ as well.

The above extension of the domain using the symmetry imposed by the boundary conditions allows us to consider each grid point with $i = 1, ..., I - 1$ and $j = 1, \ldots, J - 1$ as an inner point.

## A.2. Numerical scheme for slime molds

For each time step, the equation for the chemical $S$ is solved first. In order to do this, we use the concept of operator splitting: the diffusion term in (22) is solved using a standard alternating direction implicit method (ADI, see for instance Morton [21]). The reaction term is then computed by

$$S_{i,j}^{n+1} = \frac{\alpha k}{1 + k} u_{i,j}^n + \frac{1}{1 + k} S_{i,j}^*, \qquad (38)$$

where $S_{i,j}^*$ is the solution of the diffusion equation. The cell flux $q$ is computed by

$$q1_{i,j}^{n+1} = \frac{\tau}{(\tau + k)} q1_{i,j}^n - \frac{Dk}{2h(\tau + k)} \left( u_{i+1,j}^n - u_{i-1,j}^n \right) + \frac{k}{(\tau + k)} f1_{i,j}, \quad (39)$$

$$q2_{i,j}^{n+1} = \frac{\tau}{(\tau + k)} q2_{i,j}^n - \frac{Dk}{2h(\tau + k)} \left( u_{i,j+1}^n - u_{i,j-1}^n \right) + \frac{k}{(\tau + k)} f2_{i,j}, \quad (40)$$

with $i = 1, \ldots, I - 1$, $j = 1, \ldots, J - 1$. On the boundaries, we again have (36) and (37). Here $(f1, f2)$ denotes the chemotactic part of the flux, i.e.

$$f1_{i,j} = \frac{1}{2h} u_{i,j}^n (1 - u_{i,j}^n)(S_{i+1,j}^{n+1} - S_{i-1,j}^{n+1}), \qquad (41)$$

$$f2_{i,j} = \frac{1}{2h} u_{i,j}^n (1 - u_{i,j}^n)(S_{i,j+1}^{n+1} - S_{i,j-1}^{n+1}), \qquad (42)$$

and

$$f1_{0,j} = -f1_{2,j}, \qquad f1_{I,j} = -f1_{I-2,j}, \quad j = 1, \ldots, J - 1 \qquad (43)$$

$$f2_{i,0} = -f2_{i,2}, \qquad f2_{i,J} = -f2_{i,J-2}, \quad i = 1, \dots, I-1 \qquad (44)$$

on the boundaries.

Following the idea of Lax and Wendroff, the algorithm for the population density $u$ is based on a Taylor series expansion that is truncated after the third term. In our case

$$u(t + \Delta t, x, y) = u(t, x, y) + \Delta t(-q_{1x} - q_{2y})$$
$$+ \frac{(\Delta t)^2}{2\tau} \left[ D(u_{xx} + u_{yy}) + q_{1x} + q_{2y} - f_{1x} - f_{2y} \right].$$

The corresponding difference equation is for $i = 1, \dots, I-1$, $j = 1, \dots, J-1$

$$u_{i,j}^{n+1} = u_{i,j}^n + \left( \frac{k^2}{4\tau h} - \frac{k}{2h} \right) \left( q1_{i+1,j}^{n+1} - q1_{i-1,j}^{n+1} + q2_{i,j+1}^{n+1} - q2_{i,j-1}^{n+1} \right)$$
$$+ \frac{k^2}{2\tau} \left[ \frac{D}{h^2} \left( u_{i+1,j}^n + u_{i-1,j}^n + u_{i,j+1}^n + u_{i,j-1}^n - 4u_{i,j}^n \right) \right.$$
$$\left. - \frac{1}{2h} \left( f1_{i+1,j} - f1_{i-1,j} + f2_{i,j+1} - f2_{i,j-1} \right) \right]. \qquad (45)$$

On the boundaries, we use (32) and (33).

Thus, we have all information which is necessary to solve system (20)–(22) numerically for $t > 0$. We checked numerically that, with the boundary conditions defined above, the total population size is preserved with an accuracy of nine digits.

### A.3. Numerical scheme for bacteria

The application of the numerical scheme to the model for bacteria (29)–(31) requires some minor alterations. The equation for the chemo-attractant $S$ is again approximated using operator splitting. The equation for the flux is given by (39) and (40), where now

$$f1_{i,j} = \frac{\alpha u_{i,j}^n}{2h(1 + \beta S_{i,j}^{n+1})^2} \left( S_{i+1,j}^{n+1} - S_{i-1,j}^{n+1} \right), \qquad (46)$$

$$f2_{i,j} = \frac{\alpha u_{i,j}^n}{2h(1 + \beta S_{i,j}^{n+1})^2} \left( S_{i,j+1}^{n+1} - S_{i,j-1}^{n+1} \right), \qquad (47)$$

for $i = 1, \dots, I-1$ and $j = 1, \dots J-1$ with boundary conditions (43) and (44).

Due to the production term in the $u$-equation (29), the discretization for $u$ has to be computed anew. The Taylor series expansion of $u(t + \Delta t, x, y)$ reads:

$$u(t + \Delta t, x, y) = u(t, x, y) + \left( \frac{(\Delta t)^2}{2\tau} - \Delta t \right) (q_{1x} + q_{2y}) + \Delta t \rho u \left( 1 - \frac{u}{c} \right)$$
$$+ \frac{(\Delta t)^2}{2\tau} \left( D(u_{xx} + u_{yy}) - f_{1x} - f_{2y} \right)$$
$$+ \frac{(\Delta t)^2}{2} \rho \left( 1 - \frac{2u}{c} \right) \left( -q_{1x} - q_{2y} + \rho u \left( 1 - \frac{u}{c} \right) \right).$$

Here we used $u_t = -q_{1x} - q_{2y} + \rho u(1 - \frac{u}{c})$ and $u_{tt} = -q_{1xt} - q_{2yt} + \rho u_t (1 - \frac{2u}{c})$. The corresponding difference equation for $i = 1, \dots, I - 1$, $j = 1, \dots, J - 1$ reads

$$
\begin{aligned}
u_{i,j}^{n+1} = u_{i,j}^n &+ \left( \frac{k^2}{4\tau h} - \frac{k}{2h} \right) \left( q1_{i+1,j}^{n+1} - q1_{i-1,j}^{n+1} + q2_{i,j+1}^{n+1} - q2_{i,j-1}^{n+1} \right) \\
&+ k\rho u_{i,j}^n \left( 1 - \frac{u_{i,j}^n}{c} \right) + \frac{k^2}{2\tau} \left[ \frac{D}{h^2} (u_{i+1,j}^n + u_{i-1,j}^n + u_{i,j+1}^n + u_{i,j-1}^n - 4u_{i,j}^n) \right. \\
&\left. - \frac{1}{2h} \left( f1_{i+1,j} - f1_{i-1,j} + f2_{i,j+1} - f2_{i,j-1} \right) \right] \\
&- \frac{k^2 \rho}{2} \left( 1 - \frac{2u_{i,j}^n}{c} \right) \left( \frac{1}{2h} \left( q1_{i+1,j}^{n+1} - q1_{i-1,j}^{n+1} + q2_{i,j+1}^{n+1} - q2_{i,j-1}^{n+1} \right) \right. \\
&\left. - \rho u_{i,j}^n \left( 1 - \frac{u_{i,j}^n}{c} \right) \right).
\end{aligned}
$$

As before, we apply (32) and (33) on the boundary.

## References

1. Berg, H.: *Random Walks in Biology*. University Press, Princeton, NJ, USA, 1983
2. Berg, H.C., Brown, D.A.: Chemotaxis in Escherichia coli. analysis by three-dimensional tracking. Nature **239**, 500–504 (1972)
3. Berg, H.C., Turner, L.: Chemotaxis of bacteria in glass capillary arrays. Biophys. J. **58**, 919–930 (1990)
4. Cattaneo, C.: Sulla conduzione de calore. Atti del Semin. Mat. e Fis. Univ. Modena **3**, 83–101 (1948)
5. Dahlquist, F.W., Lovely, P., Koshland, D.E. Jr: Qualitative analysis of bacterial migration in chemotaxis. Nature, New Biol. **236**, 120–123 (1972)
6. Dunn, G.A.: Conceptual problems with kinesis and taxis. In *Symp. 46*, 1–13. Soc. Gen. Micro., 1990
7. Dworkin, M., Segel, K.H.: Solubility and diffusion coefficient of adenosine 3',5' monophosphate. J. Biol.Chem. **252**, 864–865 (1977)
8. Firtel, R.: Dictyostelium cinema. *http://www-biology.ucsd.edu/∼firtel/movies.html*, 2001
9. Ford, R.M., Lauffenburger, D.A.: Measurement of bacterial random motility and chemotaxis coefficients: II. application of single cell based mathematical model. Biotechnol. Bioeng. **37**, 661–672 (1991)
10. Ford, R.M., Phillips, B.R., Quinn, J.A., Lauffenburger, D.A.: Measurement of bacterial random motility and chemotaxis coefficients: I. stopped-flow diffusion chamber assay. Biotechnol. Bioeng. **37**, 647–660 (1991)

11. Gurtin, M.E., Pipkin, A.C.: A general theory of heat conduction with finite wave speed.
    Arch. Rational Mech. Anal. **31**, 113–126 (1968)
12. Hadeler, K.P.: Reaction telegraph equations and random walk systems. In S.J. van Strien
    and S.M. Verduyn Lunel, editors, *Stochastic and Spatial Structures of Dynamical Sys-
    tems*. Royal Academy of the Netherlands, 1995
13. Hillen, T.: Qualitative analysis of semilinear Cattaneo equations. Math. Models Meth.
    Appl. Sci. **8**(3), 507–519 (1998)
14. Hillen, T.: *Transport Equations and Chemosensitive Movement*. University of Tübingen,
    2001. Habilitation thesis
15. Hillen, T., Levine, H.: Blow-up in hyperbolic models for chemosensitive movement in
    $1 - D$. 2002. in preparation
16. Hillen, T., Painter, K.: Global existence for a parabolic chemotaxis model with preven-
    tion of overcrowding. Adv. Appl. Math. **26**(4), 280–301 (2001)
17. Hillen, T., Stevens, A.: Hyperbolic models for chemotaxis in 1-D. Nonlinear Anal.: Real
    World Appl. **1**, 409–433 (2000)
18. Joseph, D.D., Preziosi, L.: Heat waves. Rev. Mod. Phys. **61**, 41–73 (1988)
19. Keller, E.F., Segel, L.A.: Initiation of slime mold aggregation viewed as an instability.
    J. Theor. Biol. **26**, 399–415 (1970)
20. Lapidus, R., Schiller, R.: Model for the chemotactic response of a bacterial population.
    Biophys. J. **16**, 779–789 (1976)
21. Morton, K.W., Mayers, D.F.: *Numerical Solution of Partial Differential Equations*.
    Cambridge University Press, 1994
22. Othmer, H.G., Dallon, J.: Models of Dictyostelium aggregation. In W. Alt, A. Deutsch,
    and G. Dunn, editors, *Dynamics of Cell and Tissue Motion*. Birkhäuser, 1996
23. Othmer, H.G., Dunbar, S.R., Alt, W.: Models of dispersal in biological systems. J. Math.
    Biol. **26**, 263–298 (1988)
24. Othmer, H.G., Schaap, P.: Oscillatory cAMP signaling in the development of Dictyos-
    telium discoideum. Comm. Theor. Biol. **5**, 175–282 (1998)
25. Patlak, C.S.: Random walk with persistence and external bias. Bull. Math. Biophys. **15**,
    311–338 (1953)
26. Pearson, K.: The problem of the random walk. Nature **72**, 294 and 342, (1905)
27. Rietdorf, J., Siegert, F., Weijer, C.J.: Analysis of optical density wave propagation and
    cell movement during mound formation in *Dictyostelium discoideum*. Devl. Biol. **177**,
    427–438 (1996)
28. Stroock, D.W.: Some stochastic processes which arise from a model of the motion of a
    bacterium. Prob. Theory and Related Fields, **28**, 305–315 (1974)
29. Tranquillo, R.T., Alt, W.: Glossary of terms concerning oriented movement. In W. Alt
    and G. Hoffmann, editors, *Biological Motion*, volume 89 of *Lect. Notes in Biomath.*,
    510–517, Heidelberg, 1990. Springer
30. Woodward, D.D., Tyson, R., Myerscough, M.R., Murray, J.D., Budrene, E., Berg, H.C.:
    Spatio-temporal patterns generated by *Salmonella typhimurium*. Biophys. J. **68**, 2181–
    2189 (1995)